Determination of the second-order nonlinear susceptibility elements of a single nanoparticle using coherent optical microscopy

2011 J. Phys. B: At. Mol. Opt. Phys. 44 015401

(http://iopscience.iop.org/0953-4075/44/1/015401)

J. Phys. B: At. Mol. Opt. Phys. **44** (2011) 015401 (6pp) doi:10.1088/0953-4075/44/1/015401

Determination of the second-order nonlinear susceptibility elements of a single nanoparticle using coherent optical microscopy

Santosh Tripathi[1], **Brynmor J Davis**[2,3], **Kimani C Toussaint Jr**[3,4] **and P Scott Carney**[1,3]

[1] Department of Electrical and Computer Engineering, University of Illinois at Urbana-Champaign, 1406 W. Green St., Urbana, IL 61801, USA
[2] Creare Inc, PO Box 71, 16 Great Hollow Road, Hanover, NH 03755, USA
[3] The Beckman Institute for Advanced Science and Technology, University of Illinois at Urbana-Champaign, 405 North Mathews Ave., Urbana, IL 61801 USA
[4] Department of Mechanical Science and Engineering, University of Illinois at Urbana-Champaign, 1206 W. Green St., Urbana, IL 61801, USA

E-mail: ktoussai@illinois.edu and carney@illinois.edu

Received 15 September 2010
Published 10 December 2010
Online at stacks.iop.org/JPhysB/44/015401

Abstract
We present a technique based on the use of coherent confocal microscopy that can be used to estimate, to within a scale factor, all of the elements of the second-order susceptibility tensor of a single pointlike nanoparticle under permutation and Kleinman symmetry. An estimate of the three-dimensional position of a nanoparticle is also obtained. A forward model for the problem is presented and a method for solving the inverse problem is demonstrated. The approach is tested through simulations which show that the position and the elements of the susceptibility tensor can be robustly retrieved using this method.

(Some figures in this article are in colour only in the electronic version)

1. Introduction

Second-harmonic generation (SHG) is a coherent second-order nonlinear optical process which produces an optical field at twice the frequency of the input (pump) field; this process occurs only in noncentrosymmetric material systems [1, 2]. The second-order nonlinear susceptibility that describes the generation of the SHG signal depends on the electronic configurations, molecular structures and alignments, and local morphologies of the system [1]. As a result, SHG has been successfully used to investigate the local molecular alignment and/or the structure in a wide variety of materials including biological tissues [3, 4], organic and inorganic crystals [5, 6], molecular materials, and surfaces and interfaces [7]. Recently, it has also been used to characterize individual nanoparticles [2, 8–18]. In one study, the orientation and the crystalline nature of the individual organic nanocrystals were inferred from the SHG signal together with the two-photon excited fluorescence [8]. In another study, three-dimensional orientation of the individual nanocrystals was determined by imaging the emitted SHG signal using a defocused imaging system [2]. To-date limited effort has been placed on determining the elements of the second-order nonlinear susceptibility tensor for individual nanoparticles. As has been demonstrated with biological samples [19], the determination of the tensor elements provides additional information about the nanoparticles and may be useful in fields such as bioimaging, sensing, drug delivery [20], and imaging [21].

In this paper, we present a technique to determine both the position and the elements of the second-order susceptibility tensor for individual nanoparticles. It utilizes a coherent confocal microscope [20] and exploits the fact that SHG is a coherent process, so that the phase and the amplitude of the

field may be obtained interferometrically [1, 7]. We assume that the particle is pointlike, that is, its structure is unresolvable on the scale of the wavelength of light [22] and that it can be characterized by a single second-order susceptibility tensor. Analysis of large particles may require a more complicated model [20]; however, the framework presented in this paper is modular and is amenable to such modifications. We also assume that the particle is fixed in position and well isolated from other particles such that there is no inter-particle interaction, and that the optical field used to characterize the particle does not interact with neighbouring particles. In a general setting, there are not enough data available to solve for all elements of the nonlinear susceptibility simultaneously. However, it is often possible to invoke symmetries of the tensor to reduce the number of free variables and resolve the remaining elements. The Kleinman symmetry [23, 24] may be invoked for nondispersive nonabsorbing media. Then the proposed technique can be used to infer the position and extract all elements of the second-order susceptibility. In the case of failure of the Kleinman symmetry, other symmetries may be invoked to similar ends [24]. Since in practice the overall scale of the data is not known precisely, the susceptibility tensor elements are estimated up to a constant scaling factor. For practical experiments, nanoparticles may be on substrates; the retrieved susceptibility in our approach is then the effective susceptibility that includes the effect of the substrate–particle interaction. The bare particle polarizability can then be inferred from the effective polarizability. In section 2 we describe the theoretical framework, and in section 3 we present results from simulations.

2. Theory

2.1. Forward model

Figure 1 shows a simplified schematic of the proposed experiment. An input beam with fundamental frequency ω (indicated in figure 1 by dashed arrows) passes through a beam splitter. Part of the beam passes through the vector beam shaper which imparts the required phase and intensity distribution to the input beam giving rise to a field $\boldsymbol{E}^{(b)}$ at the entrance pupil of the lens L_1. The beam is then refracted by L_1 which results in the field $\boldsymbol{E}^{(l)}$ at the exit pupil of the lens and a field g in the focal volume. The sample consists of a substrate supporting the nanoparticle to be characterized. As mentioned earlier, the substrate can have more than one nanoparticle; however, these nanoparticles should be sparsely distributed so that the focused beam interacts with only the nanoparticle to be characterized. The interaction of the nanoparticle with the focused optical field generates the backscattered signal $\boldsymbol{E}^{(s)}$ which consists of the optical field at both the fundamental and second harmonic (indicated in figure 1 by solid arrows), 2ω, frequencies. This signal then propagates back through L_1 and is combined with a reference SHG signal, $\boldsymbol{E}^{(r)}(2\omega)$, at the beam splitter. The SHG filter in the signal path ensures that only the second-harmonic signal is recorded at the detector. The reference SHG signal can be generated using a nonlinear crystal with a large second-order susceptibility such as beta-barium borate (BBO) or lithium triborate (LBO) [1, 6, 7, 25].

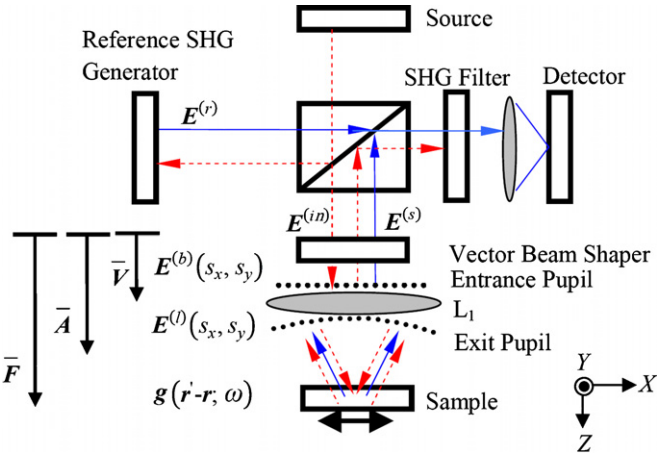

Figure 1. Schematic of the proposed experimental setup.

It should also be noted that the reference SHG signal must be generated from the illuminating optical source in order to ensure that the reference field is coherent with the SHG signal backscattered from the nanoparticle (as demonstrated in [6]).

The intensity at the detector is a function of both the position of the geometrical focus $\boldsymbol{r} = (x, y, z)$ and the second-harmonic angular frequency 2ω, and can be written as [20, 26]

$$I(\boldsymbol{r}; 2\omega) = \langle |\boldsymbol{E}^{(r)}(2\omega)|^2 \rangle + 2\,\mathrm{Re}\{S(\boldsymbol{r}; 2\omega)\} + \langle |\boldsymbol{E}^{(s)}(\boldsymbol{r}; 2\omega)|^2 \rangle, \quad (1)$$

where $\langle \ldots \rangle$ represents a time-averaging operation. In equation (1), the first term depends only on the reference signal; assuming a plane wave reference signal the dependence on $\boldsymbol{r}$ can be removed. The third term, which is the autocorrelation term, is typically very small and can usually be neglected [20]. The interferometric cross term defined as

$$S(\boldsymbol{r}; 2\omega) = \langle \{\boldsymbol{E}^{(r)}(2\omega)\}^{\dagger} \boldsymbol{E}^{(s)}(\boldsymbol{r}; 2\omega) \rangle \quad (2)$$

can be recovered from its measured real part $\mathrm{Re}\{\boldsymbol{S}(\boldsymbol{r}; 2\omega)\}$ using the Hilbert transform [20], where $\dagger$ represents the Hermitian transpose. Note that the application of the Hilbert transform in retrieving the complex field is applicable when the data are collected over a range of frequencies; alternatively, if the experiments are carried out at a single frequency, phase-shifting interferometry could be used. However, the fundamental results of this paper are independent of the technique used to retrieve the complex field.

To determine the backscattered field $\boldsymbol{E}^{(s)}(\boldsymbol{r}; 2\omega)$, we develop a forward model for the field from the incident field, through the optical system, to the interaction with the sample and back out. We denote the beam delivered by the source onto the vector beam shaper by $\boldsymbol{E}^{(\mathrm{in})}(\omega)$. It is converted to the field $\boldsymbol{E}^{(b)}(s_x, s_y; \omega)$ on the entrance pupil of the lens by the vector beam shaper, such that

$$\boldsymbol{E}^{(b)}(s_x, s_y; \omega) = \bar{\boldsymbol{V}}(s_x, s_y)\boldsymbol{E}^{(\mathrm{in})}(\omega), \quad (3)$$

Here, s_x and s_y are the components of the unit vector directed from a point on the exit pupil to the geometrical focus [27, 28] which can be mapped to a corresponding point on the entrance pupil by ray tracing, where $\bar{\boldsymbol{V}}(s_x, s_y)$ is a tensor operator

describing the operation of the vector beam shaper. Assuming an aplanatic lens obeying the sine condition and the intensity law [28], the refracting action of the lens can be written as

$$\boldsymbol{E}^{(l)}(s_x, s_y; \omega) = \bar{\boldsymbol{A}}(s_x, s_y)E^{(\mathrm{in})}(\omega), \tag{4}$$

where the tensor $\bar{\boldsymbol{A}}$ includes both the effect of the vector beam shaper and the refraction by the lens. This can be obtained from the rotation of equation (2.23) in [29] or from equation (3.51) in [28]. The field at an arbitrary point $\boldsymbol{r}'$ is calculated as [20, 27, 28]

$$\begin{aligned} g(\boldsymbol{r}' - \boldsymbol{r}; \omega) &= \frac{k}{2\pi \mathrm{i}} \int \mathrm{d}s_x \, \mathrm{d}s_y \frac{\bar{\boldsymbol{A}}(s_x, s_y)\boldsymbol{E}^{(\mathrm{in})}(\omega)}{s_z(s_x, s_y)} \, \mathrm{e}^{\mathrm{i}k\boldsymbol{s}\cdot(\boldsymbol{r}'-\boldsymbol{r})} \\ &= \bar{\boldsymbol{F}}(\boldsymbol{r}' - \boldsymbol{r}; \omega)\boldsymbol{E}^{(\mathrm{in})}(\omega), \end{aligned} \tag{5}$$

where $\bar{\boldsymbol{F}}$ is a tensor that includes the effect of the vector beam shaper and the lens. The parameter s_z, in free space, is related to s_x and s_y through the standard relation $s_z = \sqrt{1 - s_x^2 - s_y^2}$ [20]. The angular spectrum representation approach outlined here can also be modified to allow for situations where the field is focused onto a sample with background index mismatch [28].

Assuming that the nanoparticle is at a position $\boldsymbol{r}^{(p)}$ (p represents the position of the nanoparticle) and its effective 3×6 susceptibility tensor in contracted notation, i.e. the second-order susceptibility tensor under permutation symmetry, is represented by $\boldsymbol{d}$, the resultant second-harmonic polarization may be written as [23, 30]

$$\boldsymbol{P}(2\omega) = \boldsymbol{d} \begin{bmatrix} g_x^2(\boldsymbol{r}^{(p)} - \boldsymbol{r}; \omega) \\ g_y^2(\boldsymbol{r}^{(p)} - \boldsymbol{r}; \omega) \\ g_z^2(\boldsymbol{r}^{(p)} - \boldsymbol{r}; \omega) \\ 2g_y(\boldsymbol{r}^{(p)} - \boldsymbol{r}; \omega)g_z(\boldsymbol{r}^{(p)} - \boldsymbol{r}; \omega) \\ 2g_x(\boldsymbol{r}^{(p)} - r; \omega)g_z(\boldsymbol{r}^{(p)} - \boldsymbol{r}; \omega) \\ 2g_x(\boldsymbol{r}^{(p)} - r; \omega)g_y(\boldsymbol{r}^{(p)} - \boldsymbol{r}; \omega) \end{bmatrix} = \boldsymbol{d} \begin{bmatrix} e_1 \\ e_2 \\ e_3 \\ e_4 \\ e_5 \\ e_6 \end{bmatrix}, \tag{6}$$

where g_x, g_y and g_z are the x, y and z components of the focal field g and e_i is shorthand for the ith-row element of the 1×6 vector of products of the elements of g. The amplitude of the field resulting from this induced second-harmonic polarization is proportional to $k^2\boldsymbol{P}(2\omega)$ [26]. This field propagates back through the lens. By reciprocity, this operation can be described by $\bar{\boldsymbol{F}}^T(2\omega)$ [20], where T refers to the transpose of the operator. Hence, the backscattered second-harmonic field can be written as

$$\boldsymbol{E}^{(s)}(\boldsymbol{r}; 2\omega) \propto k^2 \bar{\boldsymbol{F}}^T(\boldsymbol{r}^{(p)} - \boldsymbol{r}; 2\omega)\boldsymbol{P}(2\omega). \tag{7}$$

Note that $\bar{F}$ implicitly includes the dyadic Green's function which is frequency dependent [27, 31]. It should be noted that there is a backscattered fundamental field as well; however, it is neglected since it is filtered out. The backscattered field then interferes with the reference field. Using equation (2), the complex field can be written as

$$S(\boldsymbol{r}; 2\omega) \propto k^2 \langle \{\boldsymbol{E}^{(r)}(2\omega)\}^\dagger \bar{\boldsymbol{F}}^T(\boldsymbol{r}^{(p)} - \boldsymbol{r}; 2\omega)\boldsymbol{P}(2\omega) \rangle. \tag{8}$$

Thus, one can acquire an image by fixing the focal plane at $z = 0$ and scanning the stage in two dimensions in (x, y). The received complex field, using the Einstein summation notation, can be written as

$$S(x, y; 2\omega) \propto d_{ij}(\omega)\, h_{ij}\left(x - x^p, y - y^p; z^{(p)}, 2\omega\right), \tag{9}$$

where h_{ij} are optical response functions (ORFs) which help discriminate the output signal due to each susceptibility element and are defined as

$$h_{ij}\left(x, y; z^{(p)}, 2\omega\right) = k^2 E_l^{(r)*}(2\omega) F_{il}\left(-x, -y; z^{(p)}, 2\omega\right) e_j. \tag{10}$$

In equation (10) the Einstein summation notation has again been used and * represents the complex conjugate. Also, the subscripts $i, l = 1, 2, 3$, and $j = 1, \ldots, 6$ represent the corresponding elements of the parent tensor/vector. For example, F_{12} represents an element of the first row and second column of the operator $\bar{\boldsymbol{F}}$. As equation (6) shows e_j s are the functions of the nanoparticle position. From equation (9), one sees that although the backscattered second-harmonic signal is a second-order function of the input field (through e_j), it is linearly dependent on the susceptibility elements. The ORFs defined in equation (10) are general. As noted above, it is not possible to solve for the elements of the susceptibility in the general case, and so some prior constraint must be applied. Here we invoke the Kleinman symmetry as an example, which can be enforced when $\boldsymbol{d}$ is taken to have the following form [23]:

$$\boldsymbol{d} = \begin{bmatrix} d_{11} & d_{12} & d_{13} & d_{14} & d_{15} & d_{16} \\ d_{16} & d_{22} & d_{23} & d_{24} & d_{14} & d_{12} \\ d_{15} & d_{23} & d_{33} & d_{23} & d_{13} & d_{14} \end{bmatrix}. \tag{11}$$

Equation (9) constitutes the forward model and can be used to predict the recorded signal when both the position $\boldsymbol{r}^{(p)}$ and the effective second-order susceptibility matrix $\boldsymbol{d}$ of the nanoparticle are known.

2.2. *Inverse problem*

To estimate the nanoparticle parameters, namely the susceptibility elements and the position of the particle, from the collected data, the inverse problem needs to be solved. This is achieved by searching for the set of parameters that leads to the smallest deviation between the observed data and that predicted from the forward model. There are several different quantitative metrics to estimate the deviation; in this paper, we use the Euclidian norm

$$\begin{aligned} &C(d, r^{(p)}; 2\omega) \\ &\quad = \|S(\boldsymbol{\rho}; 2\omega) - d_{ij}(\omega)h_{ij}(x - x^p, y - y^p; z^{(p)}, 2\omega)\|. \end{aligned} \tag{12}$$

The Euclidian norm chosen in equation (12) is consistent with a Gaussian noise model [32] characteristic of interferometer measurements dominated by the noise from the reference beam and/or from the thermal detector [33]. The information about the position and the susceptibility of the nanoparticle is encoded in the recorded signal through the ORFs in equation (10); therefore, successful retrieval of these parameters, as in any coding/decoding process, depends on

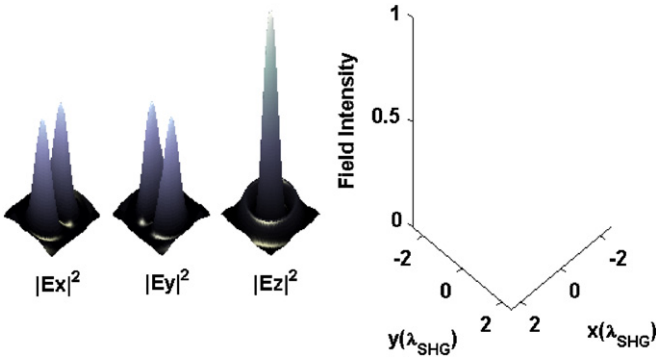

Figure 2. The intensity of each polarization component at the focal plane with the input beam and the lens parameters specified in the text. The intensities are normalized by the maximum intensity across all polarizations and all positions.

the ability of ORFs to sufficiently encode each susceptibility element onto the recorded data. Specifically, the ORFs are required to each be distinct and non-negligible. Furthermore, since the ORFs are dependent on the input field in the focal region, successful use of this technique requires that an appropriate beam type be used. For example, the focal field for a Gaussian beam contains a negligibly small field of z polarization [28]. As a result, for the Gaussian beam, several ORFs, such as h_{13} are expected to be negligible as they depend on either the z or a product of the z- and the x- or the y-polarized field in the focal region. In contrast, a strongly focused radial vector beam, a beam with polarization distribution that is radially pointing outward from the beam centre at each point [34], is also not expected to be a good choice for this technique because under very strong focusing a radial vector beam provides a strong z-polarized field at the expense of the x- and the y-polarized field [28]. In this case, ORFs such as h_{11} and h_{12} are expected to be negligible as they depend either on the x or the y field, or a product of the z- with the x- or the y-polarized field. In this paper, we choose a modified radial beam that is focused using a 0.8 numerical-aperture lens. The vector beam generator used in this paper blocks the central portion of the input beam and rotates the polarization at other points by an angle equal to the azimuthal angle of the point. Example techniques to generate such beams include the use of spiral phase delay plates, graded transmission filter [35], and spatial light modulators [36]. The resulting focal field distribution has comparable x, y, and z polarization field strengths (see figure 2) which cannot be achieved by using a uniformly polarized Gaussian beam. Figure 3 shows the real and imaginary components of the first three of the ten independent spatial domain ORFs, using the modified radial beam, when the reference field is linearly polarized along the x axis.

3. Simulations

To analyse the performance of the proposed technique numerical experiments were carried out. The nanoparticle parameters were generated randomly. One set of position values is shown below:

$$\boldsymbol{r}^{(p)} = \lambda_{\mathrm{SHG}}[-0.0139 \quad -0.1774 \quad -0.0241]^T. \tag{13}$$

The Kleinman symmetry assumes (optical) transparency [23], and as such the susceptibility elements should be real. An example of this is shown below where the values have been normalized by the maximum value:

$$\boldsymbol{d} = \begin{bmatrix} 0.8274 & 0.5416 & 0.2956 & 0.0378 & 1.0000 & 0.7854 \\ 0.7854 & 0.6721 & 0.5913 & 0.7503 & 0.0378 & 0.5416 \\ 1.0000 & 0.7503 & 0.1569 & 0.5913 & 0.2956 & 0.0378 \end{bmatrix}. \tag{14}$$

The position $\boldsymbol{r}^{(p)}$ and the contracted susceptibility matrix $\boldsymbol{d}$ were then used in equation (9) to generate the synthetic data. It consisted of a 2D complex-field distribution $S(x, y; 2\omega)$. In addition, since the data collected in actual experiments are never noise free, we choose to add complex random Gaussian noise. To generate an image with a given value of signal to noise ratio (SNR), for each pixel, the noise level is randomly chosen from a Gaussian distribution with mean and variance defined by both the signal level at that pixel and the required SNR. Specifically, the real and the imaginary parts of the complex noise are generated independently from a Gaussian distribution whose variance is equal to half of the signal power ratio to the SNR. The power at each pixel is calculated as the square of the amplitude of the complex signal at that pixel.

To solve the inverse problem, the Nelder–Mead algorithm was applied over the particle position through the *fminsearch* function in MATLAB. The initialization point for the algorithm was randomly generated using the *rand* function in MATLAB with a range of $1.5\lambda_{\mathrm{SHG}}$ in the x- and y-direction centred on the origin. During each iteration, the corresponding elements of the susceptibility were calculated using matrix inversion of the data in equation (9). Without any restriction, *fminsearch* will converge to complex values. However, requiring the susceptibility to be real at the start of the optimization procedure derails convergence as this constraint introduces discontinuity in the objective function whereas *fminsearch* assumes continuous objective function. We circumvent this problem by permitting complex values at the beginning of the optimization procedure and restricting the susceptibility to be real once a minimum is approached.

For an SNR of 25 dB, the following values of position

$$\hat{\boldsymbol{r}} = \lambda_{\mathrm{SHG}}[-0.0141 \quad -0.1767 \quad -0.0239]^T \tag{15}$$

and susceptibility elements

$$\hat{\boldsymbol{d}} = \begin{bmatrix} 0.8223 & 0.5325 & 0.2972 & 0.0342 & 1.0000 & 0.7813 \\ 0.7813 & 0.6690 & 0.5867 & 0.7451 & 0.0342 & 0.5325 \\ 1.0000 & 0.7451 & 0.1518 & 0.5867 & 0.2972 & 0.0342 \end{bmatrix} \tag{16}$$

were estimated. Again retrieved values have been normalized by the maximum real part. In practical systems the absolute scale of the data will not be known precisely—hence the normalization is for comparison purposes—so the susceptibility is estimated to within a constant scaling. We observe that the estimated value of the position closely matches the expected value (equation (13)) despite the noise. Also, comparing the elements of matrix $\hat{\boldsymbol{d}}$ with

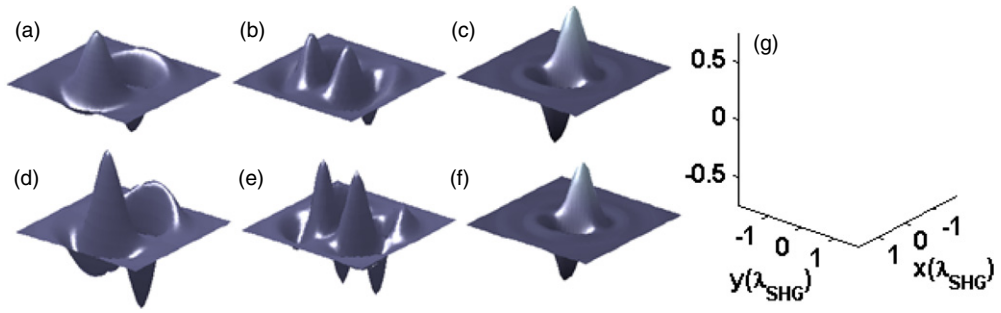

Figure 3. The real (a)–(c) and the imaginary (d)–(f) parts of the first three (of ten) spatial domain ORFs, h_{11}, h_{12}, h_{13}, for a radial vector beam at a defocus of $0.125\lambda_{\mathrm{SHG}}$ where $\lambda_{\mathrm{SHG}} = 2\pi c/2\omega$. These ORFs are dependent on the input beam type as well as on the amount of defocus, and encode the position and the susceptibility information of the nanoparticle onto the recorded signal. Thus, these ORFs can also be thought of as the basis elements, albeit non-orthogonal, onto which the measured field can be decomposed. The coefficients of the decomposition give us the ten independent elements of the second-order susceptibility tensor under the permutation and Kleinman symmetry. (g) The scales used for these plots. Here, the axes have been labelled in the units of wavelength and the ORF values have been normalized by the maximum value across all ORFs.

elements of matrix $\boldsymbol{d}$, we see that the values closely match despite the noise. It should be noted that in a physical experiment, the deduced susceptibility would be determined in the macroscopic (laboratory) reference frame. To correlate these values with the crystal structure, one will need to supplement retrieved values with knowledge of the orientation of the emission dipole (multipole) of the particle which can be obtained from techniques like defocused imaging [2].

The effect of the noise on the accuracy of the retrieved position and susceptibility is shown in figure 4. For each data point shown, numerical experiments were run ten times at a constant noise level and with a separate set of randomly generated nanoparticle parameters. The particle was restricted to the focal plane for all calculations. The error values shown are the average of the 10 error values for each point. The confocal scanning step size in the transverse direction (along x or y) and in the axial direction was $0.125\lambda_{\mathrm{SHG}}$ and $0.25\lambda_{\mathrm{SHG}}$, respectively. Figure 4(a) shows the norm of the error in the susceptibility elements. Similarly, figure 4(b) shows the Euclidian norm of the error in position $\hat{\boldsymbol{r}}^{(p)} - \boldsymbol{r}^{(p)}$ as a function of the SNR. We observe the intuitive result that as the SNR is increased the error decreases. Since only 10 of the 18 elements are independent, to calculate the norm, a vector of these 10 elements was constructed and the corresponding Euclidian norm was calculated. It again shows an improvement in the retrieval accuracy as the noise level is decreased. Although in these calculations the particle is assumed to be in the focal plane (i.e. $z = 0$), our approach allows for the position and susceptibility of the particle to be retrieved even if the particle is located in any other plane.

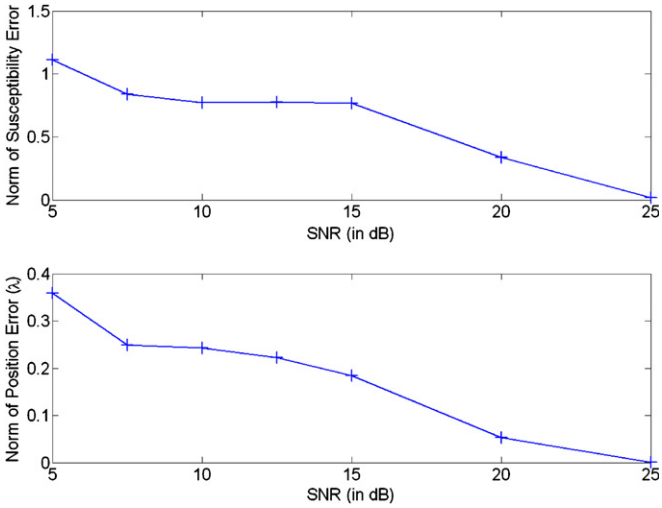

Figure 4. Euclidian norm of the error in the retrieved values of (a) the susceptibility, and (b) the position as a function of the SNR ratio. Refer to the text for details.

4. Summary

We presented a technique to determine both the position and the second-order nonlinear susceptibility tensor elements for single nanoparticles under the permutation and Kleinman symmetry. The performance of the technique was assessed through the numerical experiments which showed that the retrieval is robust. Since the nanoparticles are placed on a substrate, the retrieved values of the susceptibility will be 'effective values' in the sense that the effect of the substrate is also reflected in these values. This might be overcome by suspending the particle in a vacuum using optical levitation techniques. Furthermore, the framework presented in this paper can be extended to extract information regarding third- and higher-order susceptibilities, as well as other types of coherent interaction processes. In this paper we analysed the case of non-absorptive nanoparticles. For absorptive particles the Kleinman symmetry condition is not applicable. Although the framework developed here can be used to analyse such particles, in that case not all elements of the susceptibility tensor can be unambiguously retrieved unless some other prior conditions which reduce the number of independent susceptibility tensor elements are applicable.

Acknowledgments

This work was supported by the University of Illinois at Urbana-Champaign research start-up funds. We also thank

the reviewer for excellent comments and suggestions which improved the overall quality of the paper.

References

[1] Jiang Y, Tomov I, Wang Y and Chen Z 2004 *Opt. Lett.* **29** 1090
[2] Sandeau N, Xuan L L, Chauvat D, Zhou C, Roch J F and Brasselet S 2007 *Opt. Express* **15** 16051
[3] Yasui T *et al* 2009 *Opt. Express* **17** 912
[4] Ambekar Ramachandra Rao R, Mehta M R, Leithem S and Toussaint K C Jr 2009 *Opt. Lett.* **34** 3779
[5] Hagimoto K and Mito A 1995 *Appl. Opt.* **34** 8276
[6] Yazdanfar S, Laiho L H and So P T C 2004 *Opt. Express* **12** 2739
[7] Shaffer E, Pavillon N, Kuhn J and Depeursinge C 2009 *Opt. Lett.* **34** 2450
[8] Brasselet S *et al* 2004 *Phys. Rev. Lett.* **92** 207401
[9] Jacobsohn M and Banin U 2000 *J. Phys. Chem.* B **104** 1
[10] Brunhes T *et al* 1999 *Appl. Phys. Lett.* **75** 835
[11] Thantu N 2005 *J. Lumin.* **111** 17
[12] Delahaye E *et al* 2006 *Chem. Phys. Lett.* **429** 533
[13] Aktsipetrov O A, Elyutin P V, Fedyanin A A, Nikulin A A and Rubtsov A N 1995 *Surf. Sci.* **325** 343
[14] Bryant G W and Liu A 1999 *Superlatt. Microstruct.* **25** 361
[15] Erland J, Bozhevolnyi S I, Pedersen K, Jensen J R and Hvam J M 2000 *Appl. Phys. Lett.* **77** 806
[16] Aktsipetrov O A, Elyutin P V, Nikulin A A and Ostrovskaya E A 1995 *Phys. Rev.* B **51** 17591
[17] Djurisic A B and Leung Y H 2006 *Small* **2** 944
[18] Zielinski M, Oron D, Chauvat D and Zyss J 2009 *Small* **5** 2835
[19] Chen W L *et al* 2009 *Appl. Phys. Lett.* **94** 183902
[20] Davis B J and Carney P S 2008 *J. Opt. Soc. Am.* A **25** 2102
[21] Citrin D S 2010 *Phys. Rev.* B **81** 241413
[22] De Vries P, Van Coevorden D V and Lagendijk A 1998 *Rev. Mod. Phys.* **70** 447
[23] Boyd R 2003 *Nonlinear Optics* (San Diego, CA: Academic)
[24] Dailey C A, Burke B J and Simpson G J 2004 *Chem. Phys. Lett.* **390** 8
[25] Le Xuan L *et al* 2006 *Appl. Phys. Lett.* **89** 121118
[26] Saleh B E A and Teich M C 2007 *Fundamentals of Photonics* (Hoboken, NJ: Wiley)
[27] Davis B J, Schlachter S C, Marks D L, Ralston T S, Boppart S A and Carney P S 2007 *J. Opt. Soc. Am.* A **24** 2527
[28] Novotny L and Hecht B 2007 *Principles of Nano-Optics* (New York: Cambridge University Press)
[29] Richards B and Wolf E 1959 *Proc. R. Soc.* A **253** 358
[30] Butcher P N and Cotter D 2003 *The Elements of Nonlinear Optics* (Cambridge: Cambridge University Press)
[31] Tai C-T 1994 *Dyadic Green Function in Electromagnetic Theory* (Piscataway, NJ: IEEE)
[32] Kay S M 1993 *Fundamentals of Statistical Signal Processing: Estimation Theory* (Englewood Cliffs, NJ: Prentice-Hall)
[33] Leitgeb R, Hitzenberger C K and Fercher A F 2003 *Opt. Express* **11** 889
[34] Tripathi S and Toussaint K C 2009 *Opt. Express* **17** 21396
[35] Tidwell S C, Ford D H and Kimura W D 1990 *Appl. Opt.* **29** 2234
[36] Maurer C, Jesacher A, Fürhapter S, Bernet S and Ritsch-Marte M 2007 *New J. Phys.* **9** 78